Nanoscale

Cite this: *Nanoscale*, 2011, **3**, 4307

www.rsc.org/nanoscale

PAPER

A molecular dynamics study of the mechanical properties of graphene nanoribbon-embedded gold composites

Shih-Kai Chien, Yue-Tzu Yang and Cha'o-Kuang Chen*

Received 23rd June 2011, Accepted 2nd August 2011
DOI: 10.1039/c1nr10664c

Molecular dynamics simulations were performed to investigate the mechanical properties of a single-crystal gold nanosheet and graphene nanoribbon-embedded gold (GNR/Au) composites for various embedded locations, temperatures, and lengths. The computational results show that the Young's modulus, tensile strength, and fracture strain of GNR/Au composites are much larger than those of pure gold. The mechanical properties of GNR/Au composites deteriorate drastically due to C–C bond breaking. Thermal fluctuation and an increase in length can decrease the mechanical properties of GNR/Au composites.

1. Introduction

Graphene, a single sheet of carbon atoms, has recently been isolated from bulk graphite.[1] Graphene nanoribbons (GNRs), quasi-one-dimensional nanostructures, and narrow (typically <20 nm) strips of graphene are all promising materials for nanoelectronic applications. An increasing number of studies have focused on graphene's extraordinary physical, chemical, and mechanical properties.[2–4] For example, the electrical mobility and thermal sp^2 conductivity of graphene are over an order of magnitude greater than those of silicon.[5,6] The high electron mobility of GNRs makes them a promising candidate for the next generation of logic devices.[7] GNRs also have potential for use as chemical sensors due to their exceptional sensitivity.[8] Graphene is also an attractive material for optical and optoelectrical devices due to its large optical absorptivity and widely tunable band gap.[9,10] The ultrahigh thermal conductivity of graphene has been extensively studied both theoretically[11,12] and experimentally.[13–15] Results show that graphene is an ideal material for thermal (phononic) devices.[16,17]

The superior mechanical properties of graphene[4] make it ideally suited for nanoelectromechanical system (NEMS) applications and as reinforcing fibers in super-strong composites. Metals have become increasingly used as a matrix material for composites.[18,19] Carbon nanotubes (CNTs) have also been considered for such applications. The Young's modulus of CNT–gold composites is much larger than that of pure gold.[18] However, it is virtually impossible to obtain perfect CNTs. Defects, which influence the physical and mechanical properties, inevitably form during the growth of CNTs. Although a larger volume fraction of defective nanotubes can slightly increase the failure stress of nanocomposites, the failure strain always decreases.[20] Many GNR properties are similar to those exhibited by CNTs. The single atomic layer of GNRs, either in aligned or nonaligned form, is advantageous for making composite materials. The mechanical properties of GNRs have been extensively studied. However, there is a lack of information on the mechanical properties of GNR composites. To obtain high-performance composite materials, it is important to study the mechanical behaviors of metal-matrix composites with GNRs.

The present work reports the mechanical properties of armchair GNR (AGNR) and zigzag GNR (ZGNR) gold composites. Five models are investigated, namely inner AGNR–gold (AGNR/Au) composites, outer AGNR–gold composites, inner ZGNR–gold (ZGNR/Au) composites, outer ZGNR–gold composites, and a single-crystal gold nanosheet, under uniaxial tension using molecular dynamics (MD) simulations. Various temperatures are considered to study the thermal kinetic effect on AGNR/Au and ZGNR/Au composites. The length effects of AGNR/Au and ZGNR/Au composites are also studied. It was found that it is difficult for a perfect sp^2 graphene structure to form strong bonds with a metal matrix. Only nonbonded interatomic interaction, *i.e.*, van der Waals energy, is considered at the GNR/Au interface.

2. Computational models

2.1. Molecular dynamics

The simulation model of a single-crystal gold nanosheet was arranged to have an ideal lattice, as shown in Fig. 1(a). The crystal orientation was [100, 010, 001]. The models of the inner AGNR/Au composites, outer AGNR/Au composites, inner ZGNR/Au composites, and outer ZGNR/Au composites are shown in Fig. 1(b)–(e), respectively. The inner GNR/Au composites mean that the GNR is embedded between two gold

Department of Mechanical Engineering, National Cheng Kung University, No.1, University Road, 70101 Tainan, Taiwan. E-mail: ckchen@mail.ncku.edu.tw; Fax: +886 6 2342081

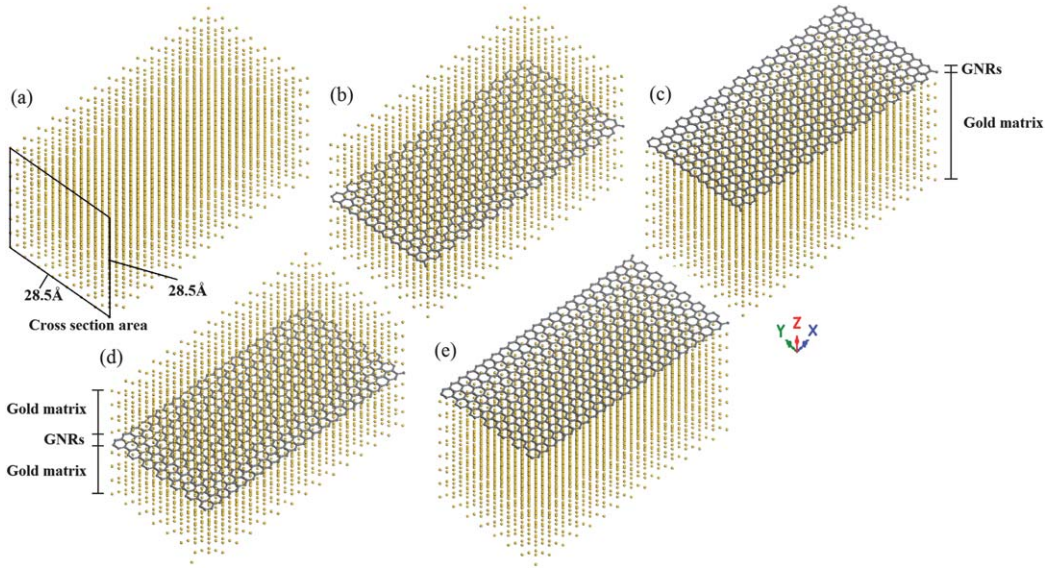

Fig. 1 Initial configurations of (a) single-crystal gold nanosheet, (b) inner AGNR/Au composites, (c) outer AGNR/Au composites, (d) inner ZGNR/Au composites, and (e) outer ZGNR/Au composites. The yellow and black atoms denote gold and carbon, respectively.

matrixes along the [100] direction; the outer GNR/Au composites mean that the GNR is embedded on the surface of gold matrix along the [100] direction. The single-crystal gold nanosheet and GNR/Au composites had cross-section areas (*yz*-plane) of around 28.5 Å × 28.5 Å, as shown in Fig. 1. All the simulations were carried out using the classical MD method, and no periodic boundary conditions were applied. Before MD calculations, the initial configuration structures were fully optimized. The velocity Verlet method was employed to integrate the equation of motion with a fixed time step of 0.5 fs. The simulations were carried out at a constant temperature (1 K, 100 K, 300 K, 600 K, and 1000 K). A 3.0 ns Nosé-Hoover thermostat coupling was used to equilibrate the system. After equilibration, the uniaxial tensile loading with a strain rate of 0.0005 ps^{-1} in the *x*-direction was applied at both ends and relaxed for 2000 steps to reach a new equilibrium state in each loading step. Loading in the *x*-direction means that the single-crystal gold nanosheet and GNR/Au composites underwent tensile deformation. Simulations were performed using the LAMMPS MD package.[21]

2.2. Graphene nanoribbons

The adaptive intermolecular reactive bond order (AIREBO) potential[22] was employed to describe C–C bonding interactions. The potential energy of a set of covalently bonded carbon atoms is given by:

$$E = \sum_i \sum_{j(>i)} \left[V^{\mathrm{R}}(r_{ij}) - b_{ij} V^{\mathrm{A}}(r_{ij}) \right] \quad (1)$$

where r_{ij} is the distance between atoms *i* and *j*, V^{R} and V^{A} are pair-wise interactions that represent the interatomic repulsions and attractions, respectively, and b_{ij} is the bond order parameter that depends on the many-body interactions between atoms *i* and *j*. This potential allows for covalent bond breaking and creation with associated changes in the hybridization of atomic orbitals within a classical potential.[23]

2.3. GNR/Au composites

The expression for the total energy of a GNR/Au composite cell can be written as:

$$E_{\mathrm{total}} = E_{\mathrm{GNR}} + E_{\mathrm{Au}} + E_{\mathrm{LJ}} \quad (2)$$

where E_{total} is the total potential energy of the GNR/Au composites, and E_{GNR} is the potential of the embedded GNRs (calculated from eqn (1)). The gold systems were modeled using the embedded-atom method potential function:[24–26]

$$E_{\mathrm{Au}} = F\left(\sum_{j \neq i} \rho(r_{ij}) \right) + \frac{1}{2} \sum_{j \neq i} \phi(r_{ij}) \quad (3)$$

where r_{ij} is the distance between atoms *i* and *j*, *F* is the embedding energy which is a function of the atomic electron density ρ, and ϕ is a pairwise potential interaction.

Since there is only a weak nonbonded interaction between carbon atoms and gold atoms, the Lennard-Jones potential was used to describe it:

$$E_{\mathrm{LJ}} = 4\varepsilon \left[\left(\frac{\sigma}{r} \right)^{12} - \left(\frac{\sigma}{r} \right)^{6} \right] \quad (4)$$

where ε and σ are the coefficients of the well-depth energy and the equilibrium distance, respectively. The parameters for the interactions between carbon atoms and gold atoms were obtained from ref. 27: $\varepsilon = 0.01272$ eV and $\sigma = 0.29943$ nm.

To obtain the stress–strain curves during deformation, the virial stress theorem was used. The atomic stress of individual atoms was calculated according to the equation:[28,29]

$$\sigma_{\alpha\beta} = \sigma_{\alpha\beta}^{\mathrm{kin}} + \sigma_{\alpha\beta}^{\mathrm{int}} \quad (5)$$

where α and β denote indices in a Cartesian coordinate system, $\sigma_{\alpha\beta}$ is the total virial stress, $\sigma_{\alpha\beta}^{\mathrm{kin}}$ is the kinetic part of the virial stress, and $\sigma_{\alpha\beta}^{\mathrm{int}}$ is the internal part of the virial stress. The internal part of the virial stress can be written as:

$$\sigma_{\alpha\beta}^{\mathrm{int}} = \frac{1}{\Omega}\left(\sum_{j=1,n} f_{ij}^{\alpha} r_{ij}^{\beta}\right) \tag{6}$$

where i and j are the atomic indices, Ω is the volume used to calculate the stress, f_{ij}^{α} is the force acting on atom i due to its interaction with atom j in the α direction, and r_{ij}^{β} is the distance between atoms i and j in the β direction. After obtaining the stress of each atom, we computed the stress of the single-crystal gold nanosheet and GNR/Au composites by averaging over all the atoms.

From the stress–strain curves, the Young's modulus (Y) was evaluated as the slope of the stress–strain curve at the initial tangent in the form of $Y = \mathrm{d}\sigma/\mathrm{d}\varepsilon$, in which σ is the stress and ε is the strain. The tensile strength and fracture strain were defined at the point where the maximum value of stress is reached.

3. Results and discussion

To validate the proposed approach, we investigated the mechanical behavior of the single-crystal gold nanosheet and GNR/Au composites at 1 K to avoid the thermal kinetic effect. In this case, the lengths of the single-crystal gold nanosheet and GNR/Au composites were around $L = 50$ Å in the loading direction. Fig. 2 shows the stress–strain curves for the single-crystal gold nanosheet and GNR/Au composites under axial tension. Based on the slope of the stress–strain curve, the Young's modulus of the single-crystal gold nanosheet is 54.02 GPa. The maximum stress is 6.65 GPa at a strain of 0.098. The results are in good agreement with previously reported experimental results.[30] With the mechanical properties of the single-crystal gold nanosheet validated with experimental observations, we now considered the inner AGNR/Au and outer AGNR/Au composites. It is worth noting that the Young's modulus of 890 GPa for AGNR[23] is about 16 times that (54.02 GPa) of pure gold. The Young's moduli of the inner AGNR/Au composite and the outer AGNR/Au composite are 124.95 GPa and 146.72 GPa, respectively. Similarly, the modulus of 830 GPa for ZGNR[23] is about 15 times that of pure gold. The Young's moduli of the inner ZGNR/Au composite and the outer ZGNR/Au composite are 112.23 GPa and 133.5 GPa, respectively. The Young's moduli of the outer AGNR/Au composite and the outer ZGNR/Au composite are much higher than that of pure gold. Table 1 shows that the GNR-embedded position affects the values of Young's modulus. However, the GNR-embedded position has no obvious effect on the strength and fracture strain. Table 1 also shows that the increment of the strength of the ZGNR/Au composites is larger than that of AGNR/Au composites, even though the Young's modulus and fracture strain of AGNR/Au composites are much larger than those of ZGNR/Au composites.

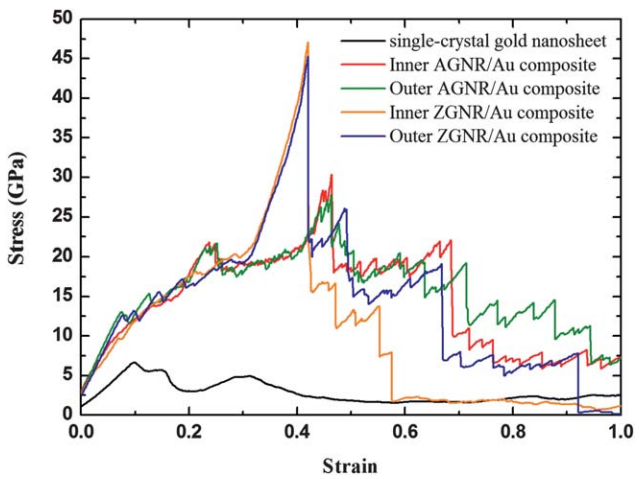

Fig. 2 Stress–strain curves of a single-crystal gold nanosheet and GNR/Au composites at 1 K.

The central cross-section layer ($x = L/2$) of the single-crystal gold nanosheet is shown in the inset of Fig. 3. The displacements of the central cross-section layer (D) is relative to the initial position and expressed as an average of 113 atoms in the central cross-section layer. The displacements of the central cross-section layer can be written as:

$$D = \frac{1}{N}\sum_{i=1,N}\sqrt{(\mathrm{d}x_i)^2+(\mathrm{d}y_i)^2+(\mathrm{d}z_i)^2} \tag{7}$$

where N is the number of atoms in the central cross-section layer, $\mathrm{d}x_i$, $\mathrm{d}y_i$ and $\mathrm{d}z_i$ are the displacements of atom i relative to the initial position in the x-, y- and z-direction, respectively. The displacements of the central cross-section layer of the single-crystal gold nanosheet and the GNR/Au composites *versus* strain are shown in Fig. 3. The displacements of the central cross-section layer of the single-crystal gold nanosheet show a significant increase when tensile loading was applied. The tensile loading ruptured the gold–gold bonds in the central cross-section layer and deformed the single-crystal gold nanosheet structure. In contrast, the atoms in the central cross-section layer in GNR/Au composites have limited interatomic force at the beginning of tensile loading. It should be noted that the displacements of the central cross-section layer of the outer AGNR/Au and the outer ZGNR/Au composites increased suddenly at strains of 0.076 and

Table 1 Mechanical properties of a single-crystal gold nanosheet and GNR/Au composites obtained from simulations at 1 K

	Young's modulus/GPa	Strength/GPa	Fracture strain
Single-crystal gold nanosheet	54.02	6.65	0.098
Inner AGNR/Au composites	124.95	30.32	0.464
Outer AGNR/Au composites	146.72	27.75	0.464
Inner ZGNR/Au composites	112.23	47.08	0.42
Outer ZGNR/Au composites	133.50	45.24	0.42

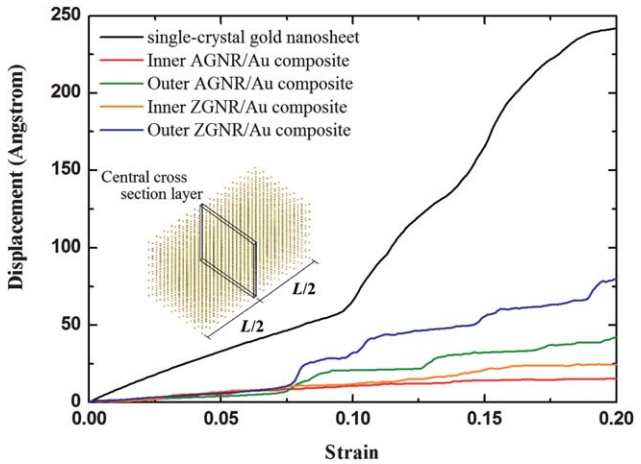

Fig. 3 Displacement *versus* strain for a central cross-section layer of a single-crystal gold nanosheet and GNR/Au composites at 1 K. The inset shows the central cross-section layer ($x = L/2$) of a single-crystal gold nanosheet.

0.078, respectively. In order to understand the rapid increase in the displacement of the central cross-section layer and to visualize the process of tensile deformation of GNR/Au composites, we consider the snapshots of the atomic arrangements of GNR/Au composites. For the inner AGNR/Au composites at a strain of 0.076 (see Fig. 4(a)), the single-crystal gold nanosheet structure experienced a dislocation near both ends; however, the GNRs did not yield completely due to the strong sp^2 bond network of GNRs. As the strain was increased until a fracture strain of 0.464, the dislocations continued to occur and propagate in the single-crystal gold nanosheet structure and sp^2 bonds began to break. Once the sp^2 bonds had broken, the dangling bonds led to the formation and propagation of cracks and the tearing of the GNRs. In all cases considered, the strength and fracture strain of the composites were dominated by the sp^2 bonds of GNRs. Fig. 4(b) shows the outer AGNR/Au composites at a strain of 0.076. It can be clearly seen that dislocations occurred in the central cross-section layer of the single-crystal gold nanosheet. These dislocations cause the atoms to abruptly move as mentioned above (see Fig. 3). When the composite was stretched to a fracture strain of 0.464, the C–C sp^2 bonds broke, causing the necking in GNRs. Fig. 4(c) and (d) show snapshots of the deformation of the inner and outer ZGNR/Au composites. The dislocations occur at a strain of 0.078, and the C–C sp^2 bonds broke at a strain of 0.42. It is interesting to note that the sp^2 bonds broke in the central cross-section layer of the outer GNR/Au composites rather than in the central cross-section

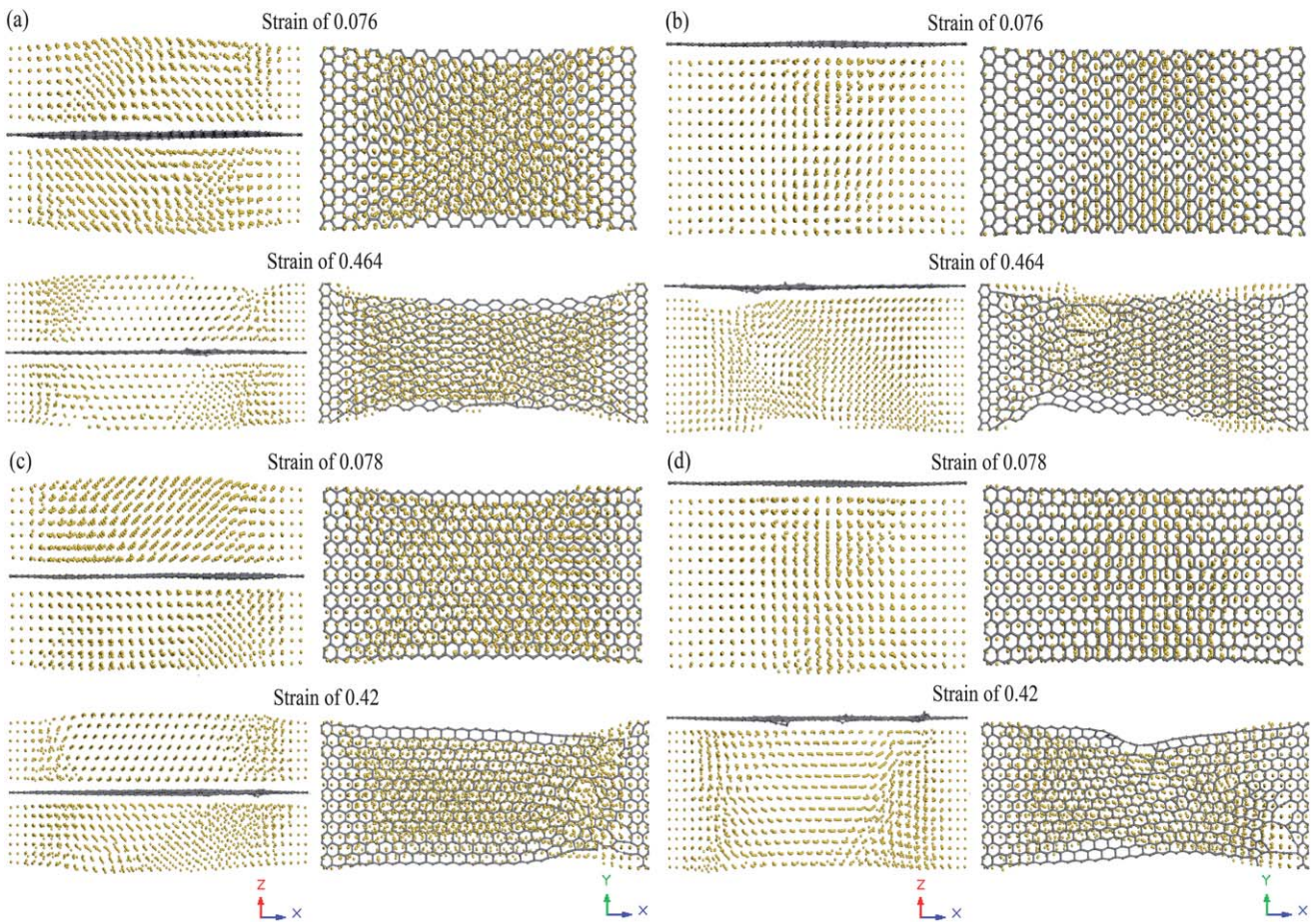

Fig. 4 Snapshots of atomic arrangements of (a) inner AGNR/Au composites, (b) outer AGNR/Au composites, (c) inner ZGNR/Au composites, and (d) outer ZGNR/Au composites at various strain values at 1 K. The yellow and black atoms denote gold and carbon, respectively.

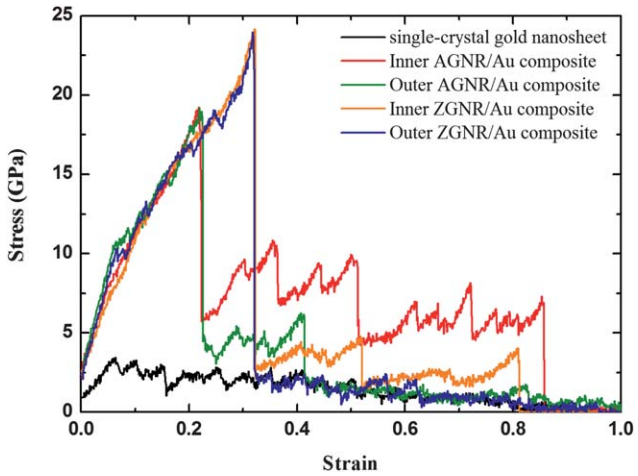

Fig. 5 Stress–strain curves of a single-crystal gold nanosheet and GNR/Au composites at 300 K.

layer of the inner GNR/Au composites. This phenomenon is due to the GNR embedded location. In the inner GNR/Au composites, there are restrictions on the dislocation of GNR that occur between two layers of the neighboring gold matrixes. In contrast, there is no such restriction on the GNR dislocation in the outer GNR/Au composites.

The thermal fluctuation affects the single-crystal gold nanosheet and GNR/Au composites that result in stress–strain curves. Fig. 5 shows the stress–stain curves for the single-crystal gold nanosheet and GNR/Au composites under uniaxial tension at 300 K. At high temperature, the velocity of the atoms increased, leading to a large thermal fluctuation. The strength and fracture strain of the single-crystal gold nanosheet and GNR/Au composites at 300 K are lower than those at 1 K. This difference in mechanical properties is attributed to the thermal fluctuations. In order to understand the decrease in Young's modulus, strength, and fracture strain with increasing temperature, the mechanical properties of GNR/Au composites obtained from extensive molecular dynamics simulations at various temperatures are shown in Fig. 6. It can be seen from Fig. 6(a) that the Young's modulus of GNR/Au composites remarkably decreases with increasing temperature. Furthermore, the Young's modulus of the outer GNR/Au composites is more sensitive to the temperature than that of the inner GNR/Au composites. A Young's modulus reduction of 40.3% was obtained at a temperature of 1000 K for the outer AGNR/Au composites, which is slightly larger than that obtained for the outer ZGNR/Au composites (39.7%). The tensile strength and fracture strain also decreased with increasing temperature. Fig. 6(b) and (c) illustrate that at a temperature of 100 K, there was a noticeable drop in both the strength and fracture strain. Surprisingly, the strength and fracture strain are less sensitive to temperature in the range of 300 K to 1000 K.

To further investigate the relationship between the mechanical properties and length of GNR/Au composites at a temperature of 1 K, they are plotted in Fig. 7. As for GNR/Au composites with a length ranging from 32 to 65 Å in the loading direction, Fig. 7(a) shows that Young's modulus slightly decreases with increasing length of the outer GNR/Au composites. A decline of

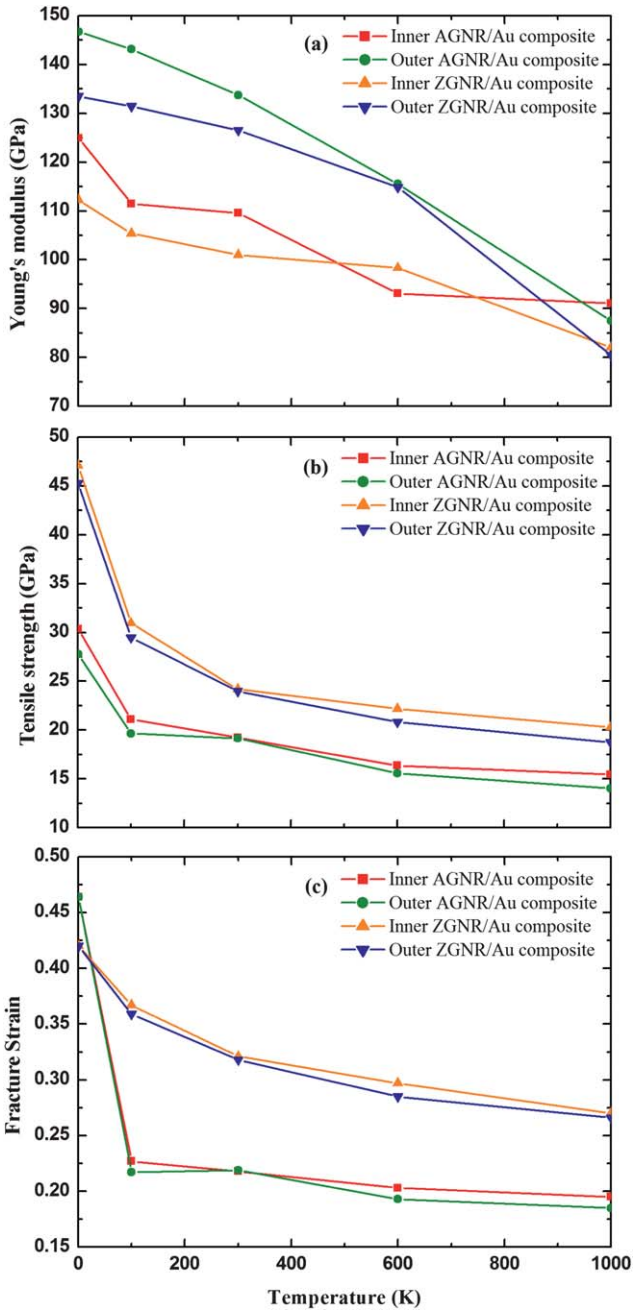

Fig. 6 Effect of temperature on (a) Young's modulus, (b) tensile strength, and (c) fracture strain of GNR/Au composites with a length of 50 Å.

only 3.7% in the Young's modulus of the outer AGNR/Au composites was found when the length increased from 32 to 65 Å. A similarly small decline (about 4.0%) in the Young's modulus of the outer ZGNR/Au composites was found when the length increased from 32 to 65 Å. In contrast, for the inner GNR/Au composites, Young's modulus is sensitive to the length. For example, the Young's modulus decreased by about 21% when the length of AGNR/Au composites increased from 40 to 65 Å, that of the ZGNR/Au composites decreased by about 15.5%. Unlike the Young's modulus, both the tensile strength and fracture strain are insensitive to the length of GNR/Au composites. Their

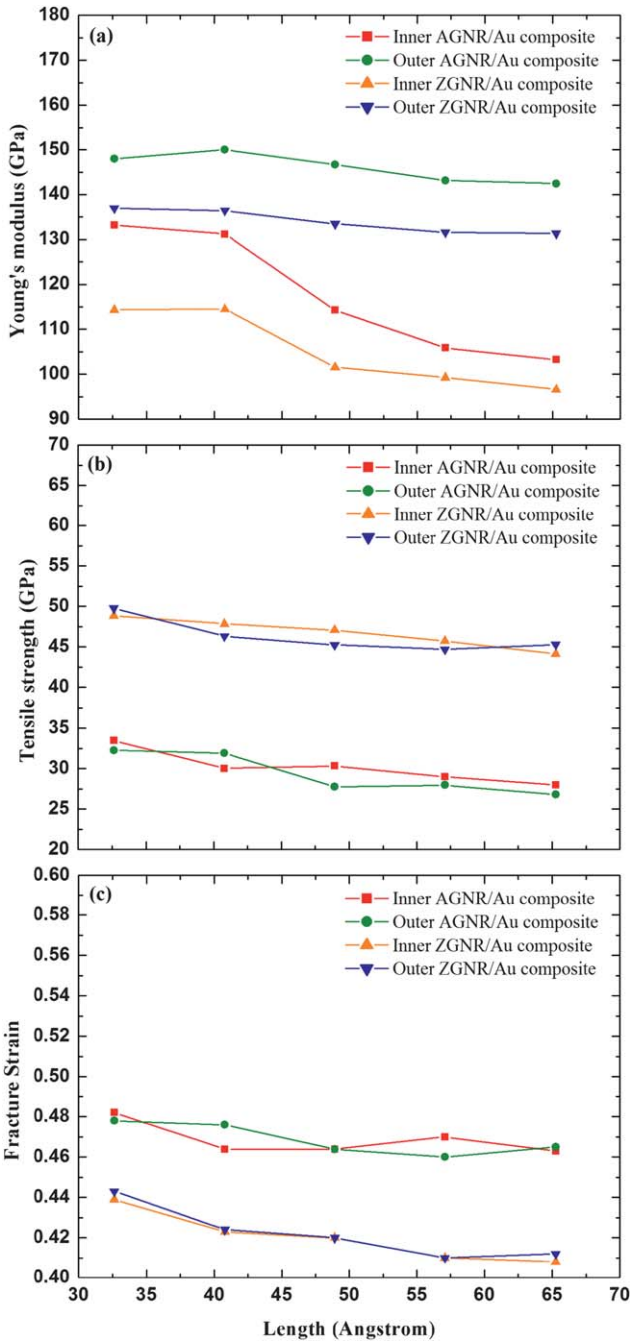

Fig. 7 Effect of GNR/Au composite length on (a) Young's modulus, (b) tensile strength, and (c) fracture strain at 1 K.

values only slightly decreased when the length of GNR/Au composites increased from 32 to 65 Å. The GNR-embedded position has no obvious effect on the strength and fracture strain.

4. Conclusion

Molecular dynamics simulations of a single-crystal gold nanosheet and GNR–gold composites were performed, and the stress–strain curves were derived. The tensile stress of 6.65 GPa and Young's modulus of 54.017 GPa of the single-crystal gold nanosheet obtained from simulations are very close to previously reported experimental results. The mechanical properties of the GNR/Au composites are better than those of the single-crystal gold nanosheet. Simulations show that the breaking of C–C sp^2 bonds contributes to the loss of strength of GNR/Au composites. In addition, a higher temperature leads to structure rupture and decreases in Young's modulus, strength, and fracture strain due to thermal fluctuation. The effect of length on the mechanical properties of GNR/Au composites was studied. The Young's modulus of the inner GNR/Au composites is sensitive to length. The inner or outer GNR-embedded position has no significant effect on the strength and fracture strain. The results suggest that the GNR–gold composites are suitable for high-performance composite materials. It is worth noting that only the weak GNR/matrix interface was considered in this study. Strong interface bonding between the graphene and the matrix may be achieved through the functionalization of graphene. This will be our future research topic.

Acknowledgements

The authors acknowledge the financial support provided by the National Science Council of Taiwan under grant NSC-99-2221-E-006-165-MY3.

References

1 K. S. Novoselov, A. K. Geim, S. V. Morozov, D. Jiang, Y. Zhang, S. V. Dubonos, I. V. Grigorieva and A. A. Firsov, *Science*, 2004, **306**, 666.
2 N. Tombros, C. Jozsa, M. Popinciuc, H. T. Jonkman and B. J. van Wees, *Nature*, 2007, **448**, 571.
3 J. S. Bunch, A. M. van der Zande, J. M. Parpia, H. G. Craighead and P. L. McEuen, *Nano Lett.*, 2008, **8**, 2458.
4 C. Lee, X. Wei, J. W. Kysar and J. Hone, *Science*, 2008, **321**, 385.
5 S. V. Morozov, K. S. Novoselov, M. I. Katsnelson, F. Schedin, D. C. Elias, J. A. Jaszczak and A. K. Geim, *Phys. Rev. Lett.*, 2008, **100**, 016602.
6 D. L. Nika, E. P. Pokatilov, A. S. Askerov and A. A. Balandin, *Phys. Rev. B: Condens. Matter Mater. Phys.*, 2009, **79**, 155413.
7 Y. M. Lin, K. A. Jenkins, A. Valdes-Garcia, J. P. Small, D. B. Farmer and P. Avouris, *Nano Lett.*, 2009, **9**, 422.
8 F. Schedin, A. K. Geim, S. V. Morozov, E. W. Hill, P. Blake, M. I. Katsnelson and K. S. Novoselov, *Nat. Mater.*, 2007, **6**, 652.
9 A. K. Geim and K. S. Novoselov, *Nat. Mater.*, 2007, **6**, 183.
10 V. Ryzhii, V. Mitin, M. Ryzhii, N. Ryabova and T. Otsuji, *Appl. Phys. Express*, 2008, **1**, 063002.
11 A. A. Balandin, S. Ghosh, W. Bao, I. Calizo, D. Teweldebrhan, F. Miao and C. N. Lau, *Nano Lett.*, 2008, **8**, 902.
12 S. Ghosh, I. Calizo, D. Teweldebrhan, E. P. Pokatilov, D. L. Nika, A. A. Balandin, W. Bao, F. Miao and C. N. Lau, *Appl. Phys. Lett.*, 2008, **92**, 151911.
13 Z. X. Guo, D. Zhang and X. G. Gong, *Appl. Phys. Lett.*, 2009, **95**, 163103.
14 J. Lan, J. W. Wang, C. K. Gan and S. K. Chin, *Phys. Rev. B: Condens. Matter Mater. Phys.*, 2009, **79**, 115401.
15 B. D. Kong, S. Paul, M. Buongiorno Nardelli and K. W. Kim, *Phys. Rev. B: Condens. Matter Mater. Phys.*, 2009, **80**, 033406.
16 N. Yang, G. Zhang and B. Li, *Appl. Phys. Lett.*, 2009, **95**, 033107.
17 J. N. Hu, X. L. Ruan and Y. P. Chen, *Nano Lett.*, 2009, **9**, 2730.
18 H. Y. Song and X. W. Zha, *Phys. B*, 2008, **403**, 559.
19 H. Y. Song and X. W. Zha, *Phys. Lett. A*, 2010, **374**, 1068.
20 S. P. Xiao and W. Y. Hou, *Phys. Rev. B: Condens. Matter Mater. Phys.*, 2006, **73**, 115406.
21 S. Plimpton, *J. Comput. Phys.*, 1995, **117**, 1.
22 D. W. Brenner, O. A. Shenderova, J. A. Harrison, S. J. Stuart, B. Ni and S. B. Sinnott, *J. Phys.: Condens. Matter*, 2002, **14**, 783.
23 Q. X. Pei, Y. W. Zhang and V. B. Shenoy, *Carbon*, 2010, **48**, 898.
24 M. S. Daw and M. I. Baskes, *Phys. Rev. Lett.*, 1983, **50**, 1285.

25 M. S. Daw and M. I. Baskes, *Phys. Rev. B*, 1984, **29**, 6443.
26 S. M. Foiles, M. I. Baskes and M. S. Daw, *Phys. Rev. B*, 1986, **33**, 7983.
27 S. Arcidiacono, J. H. Walther, D. Poulikakos, D. Passerone and P. Koumoutsakos, *Phys. Rev. Lett.*, 2005, **94**, 105502.
28 N. Chandra, S. Namilae and C. Shet, *Phys. Rev. B: Condens. Matter Mater. Phys.*, 2004, **69**, 094101.
29 T. Ragab and C. Basaran, *Comput. Mater. Sci.*, 2009, **46**, 1135.
30 J. D. Kiely and J. E. Houston, *Phys. Rev. B: Condens. Matter*, 1998, **57**, 12588.